IOP Publishing Physica Scripta
Phys. Scr. 95 (2020) 065506 (9pp) https://doi.org/10.1088/1402-4896/ab7dd4

The dispersion behaviors of the tripod-type four-level cylindrical quantum dot under phenomenon of electromagnetically induced transparency

Behjat Behroozian[1], Mohammad Reza Rezaie[2] and Hassan Ranjbar Askari[3,4]

[1] Department of Photonics, Faculty of Sciences and Modern Technologies, Graduate University of Advanced Technology, Kerman, Iran
[2] Department of Nuclear Engineering, Faculty of Sciences and Modern Technologies, Graduate University of Advanced Technology, Kerman, Iran
[3] Department of Physics, Faculty of Science, Vali-e-Asr University of Rafsanjan, Rafsanjan, Iran

E-mail: behroozian_behjat@yahoo.com, b.behroozian@student.kgut.ac.ir, mr.rezaie@kgut.ac.ir, mohamadreza45@gmail.com, hraskari@mail.vru.ac.ir and hraskarivaliasr@yahoo.com

Received 10 January 2020, revised 22 February 2020
Accepted for publication 9 March 2020
Published 2 April 2020

Abstract

In this paper, linear and 3rd-order nonlinear group velocities of the probe laser field are investigated in a tripod-type four-level cylindrical quantum dot (TTFLCQD) with parabolic potential in electromagnetically induced transparency. The nonlinear refractive index for this system is calculated by obtaining the real part of the 1st and 3rd-order susceptibilities. Afterward, linear and 3rd-order nonlinear group velocities are found. The control lasers at z-polarization are applied to the system in order to investigate the linear and 3rd-order nonlinear group velocities and the results are discussed. The linear and 3rd-order nonlinear group velocities are compared at z-polarization. Furthermore, the effects of parameters of TTFLCQD and control lasers on linear and 3rd-order nonlinear group velocities are explored. Finally, 3rd-order nonlinear group velocity for z- and x-polarization is compared.

Keywords: tripod-type cylindrical quantum dot, linear group velocity, slow light, nonlinear group velocity, electromagnetically induced transparency

(Some figures may appear in colour only in the online journal)

1. Introduction

For almost a century, control of the group velocity (v_g) has been studied quantitatively. It has been realized that the group velocity could be slower than the velocity of light in a vacuum (c) or could even be faster than c. The slow light (SL) phenomenon refers to light that propagates with group velocity much slower than c ($v_g \ll c$) [1, 2]. Recently, the slow light due to its extensive applications in low-light nonlinear optical devices [3], quantum information processing [4], optical switches [5, 6] and optical buffers [7] have attracted remarkable attention from many researchers, both theoretically and technologically. A specific physical phenomenon that laid a foundation for generating the slow light using a material dispersion in various systems is electromagnetically induced transparency (EIT) [8–10]. In this phenomenon, an absorbing atomic medium is rendered transparent by the probe laser field in the presence of one or several strong control laser fields [11–13]. EIT has a considerable application in manipulating the speed of light, particularly in achieving the slow light phenomenon [14]. Using this phenomenon, Kasapi *et al* [15] observed a group velocity of

[4] Author to whom any correspondence should be addressed.

$v_g = c/165$ in a 10-cm-long pb vapor cell. Later on, Hau *et al* [16] observed the velocity of light slow down to 17 ms^{-1} in sodium atoms steam at ultralow temperature. Evangelou *et al* [17] theoretically demonstrated that in a four level quantum system near a plasmonic nanostructure, slow light can be occurred due to the presence of plasmonic nanostructure under conditions of EIT.

More recently, experimental and theoretical studies of the slow light via EIT have been considered in semiconductor nanostructures due to their potentially important applications in optoelectronics and optical communication systems [18–22]. Yan *et al* [18] observed slow light in a V-type three-level system of GaAs/AlGaAs multiple quantum wells. 9.31×10^4 ms^{-1} and 6.5 Ps are calculated for group velocity and corresponding delay time, respectively. Quantum dots (QDs) are great candidates for EIT because of their quantized energy levels and relatively low dephasing rates [23]. Mirzaei *et al* [19] theoretically compared the group velocity of light in V-type and Λ-type three level quantum dots by EIT phenomenon. QDs coupled systems are exploited to build hybrid systems [24, 25]. EIT and slow light are investigated in the hybrid systems [26–28]. In the usual sense, the group velocity is the propagation velocity of the envelope of a pulse. The pulse can be linear, nonlinear and any other one. In this work, we called the velocity of the propagated pulse envelope as the linear and nonlinear group velocities. Here, the linear and 3rd-order nonlinear group velocities of the probe laser field are investigated in a TTFLCQD with parabolic potential in electromagnetically induced transparency. The control lasers at z-polarization are applied to system and the results are investigated. Also, linear and 3rd-order nonlinear group velocities in z-polarization are compared. The effects of parameters of TTFLCQD and control lasers on linear and 3rd-order nonlinear group velocities are investigated. Moreover, 3rd-order nonlinear group velocity in z- and x-polarization is compared.

2. The model and equations

Schematic description of the system under consideration, which is a TTFLCQD, is illustrated in figure 1(a). In figure 1(b), the diagram of the tripod-type four-level system is shown in ^{87}Rb atom [29]. The tripod-type four-level system has three ground states and one excited state. In this work, ground states are $|0\rangle$, $|1\rangle$, $|2\rangle$ and excited state is $|3\rangle$. The transitions of $|0\rangle \rightarrow |3\rangle$, $|1\rangle \rightarrow |3\rangle$ and $|2\rangle \rightarrow |3\rangle$ are three allowed transitions and $|0\rangle \rightarrow |1\rangle$, $|1\rangle \rightarrow |2\rangle$ and $|0\rangle \rightarrow |2\rangle$ are three forbidden transitions. The level $|3\rangle$ is coupled to the level $|0\rangle$ by the probe laser field with frequency ω_p and amplitude of electric field $\vec{E}_{0p}$. The levels $|2\rangle$ and $|1\rangle$ are coupled to the level $|3\rangle$ by two control laser fields with frequencies ω_{c1}, ω_{c2} and amplitude of electric fields $\vec{E}_{0c1}$, $\vec{E}_{0c2}$, respectively. The total Hamiltonian of this system in the rotating wave and dipole approximation is obtained as

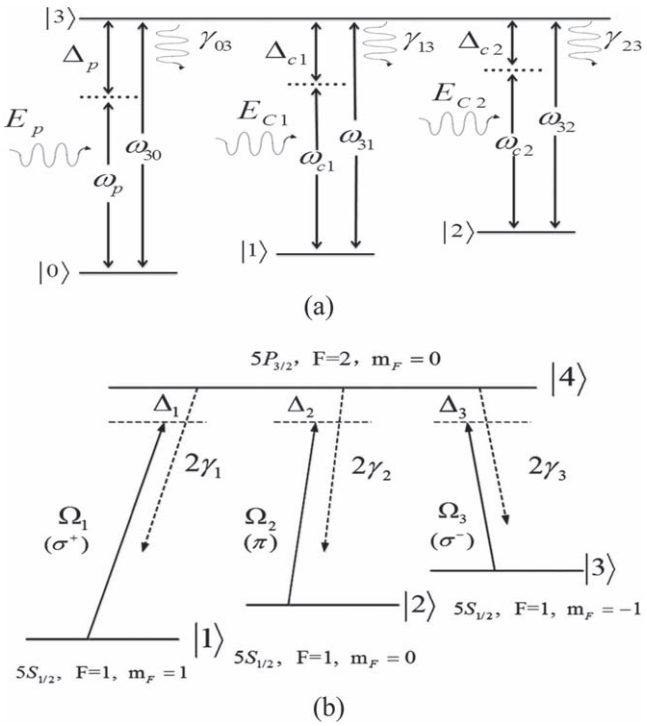

Figure 1. The diagram of the (a) tripod-type four-level system with a probe laser field and two control laser fields, (b) tripod-type four-level system in ^{87}Rb atom [29].

follows:

$$H = \frac{\hbar}{2}[2(\Delta_p - \Delta_{c1})|1\rangle\langle 1| + 2(\Delta_p - \Delta_{c2})|2\rangle\langle 2| + 2\Delta_p|3\rangle\langle 3| - (\Omega_p|0\rangle\langle 3| + \Omega_{c1}|1\rangle\langle 3| + \Omega_{c2}|2\rangle\langle 3| + H.c.)] \quad (1)$$

where $\Delta_p = \omega_p - \omega_{30}$, $\Delta_{c1} = \omega_{c1} - \omega_{31}$ and $\Delta_{c2} = \omega_{c2} - \omega_{32}$ are the detunings of the probe and control laser fields, respectively. ω_{30}, ω_{31} and ω_{32} are the atomic transition frequencies. $\Omega_p = E_{0P}|\hat{\vec{\mu}}_{03}|/\hbar$ is the complex Rabi frequency for the probe laser field, and $\Omega_{c1} = E_{0c1}|\hat{\vec{\mu}}_{13}|/\hbar$ and $\Omega_{c2} = E_{0c2}|\hat{\vec{\mu}}_{23}|/\hbar$ are the complex Rabi frequencies for the control laser fields. $\hbar$ is Planck's constant. $\hat{\vec{\mu}}_{03}$, $\hat{\vec{\mu}}_{13}$ and $\hat{\vec{\mu}}_{23}$, are the electric dipole matrix elements.

Using equation (1) and under the rotating wave approximation, the density matrix elements can be written as:

$$\dot{\rho}_{00} = \frac{i}{2}(\rho_{30} - \rho_{03})\Omega_p + \Gamma_{03}\rho_{33}$$

$$\dot{\rho}_{11} = \frac{i}{2}(\rho_{31} - \rho_{13})\Omega_{c1} + \Gamma_{13}\rho_{33}$$

$$\dot{\rho}_{22} = \frac{i}{2}(\rho_{32} - \rho_{23})\Omega_{c2} + \Gamma_{23}\rho_{33}$$

$$\dot{\rho}_{33} = \frac{i}{2}((\rho_{03} - \rho_{30})\Omega_p + (\rho_{13} - \rho_{31})\Omega_{c1} + (\rho_{23} - \rho_{32})\Omega_{c2}) - (\Gamma_{03} + \Gamma_{13} + \Gamma_{23})\rho_{33}$$

$$\dot{\rho}_{12} = \mathrm{i}(\Delta_{c1} - \Delta_{c2})\rho_{12} + \frac{i}{2}(\Omega_{c1}\rho_{32} - \Omega_{c2}\rho_{13})$$

$$\begin{aligned}
\dot{\rho}_{23} &= (i\Delta_{c2} - \gamma_{23})\rho_{23} \\
&\quad + \frac{i}{2}(-\Omega_{c1}\rho_{21} - \Omega_p\rho_{20} - \Omega_{c2}(\rho_{22} - \rho_{33})) \\
\dot{\rho}_{13} &= (\mathrm{i}\Delta_{c1} - \gamma_{13})\rho_{13} \\
&\quad + \frac{i}{2}(\Omega_{c1}(\rho_{33} - \rho_{11}) - \Omega_{c2}\rho_{12} - \Omega_p\rho_{10}) \\
\dot{\rho}_{01} &= \mathrm{i}(\Delta_p - \Delta_{c1})\rho_{01} + \frac{i}{2}(\Omega_p\rho_{31} - \Omega_{c1}\rho_{03}) \\
\dot{\rho}_{02} &= \mathrm{i}(\Delta_p - \Delta_{c2})\rho_{02} + \frac{i}{2}(\Omega_p\rho_{32} - \Omega_{c2}\rho_{03}) \\
\dot{\rho}_{03} &= (i\Delta_p - \gamma_{03})\rho_{03} \\
&\quad + \frac{i}{2}(\Omega_p(\rho_{33} - \rho_{00}) - \Omega_{c1}\rho_{01} - \Omega_{c2}\rho_{02})
\end{aligned} \tag{2}$$

$\Gamma_{ij}s$ are transition rates of the level $|i\rangle$ to level $|j\rangle$ and $\gamma_{ij}s$ are decay rates density matrix elements. By assuming the steady state and under the weak probe laser field approximation, the 1st and 3rd-order density matrix elements $\rho_{30}^{(1)}$ and $\rho_{30}^{(3)}$ can be written as [30]:

$$\rho_{30}^{(1)} = \frac{2\Omega_p(\Delta_p - \Delta_{c1})(\Delta_p - \Delta_{c2})}{(\Delta_p - \Delta_{c2})[4(\Delta_p - i\gamma_{03})(\Delta_p - \Delta_{c1}) - \Omega_{c1}^2] - \Omega_{c2}^2(\Delta_p - \Delta_{c1})} \tag{3}$$

$$\begin{aligned}
\rho_{30}^{(3)} &= \frac{\Omega_p\Omega_{c1}\rho_{13}^{(2)}(\Delta_p - \Delta_{c2}) + \Omega_p\Omega_{c2}\rho_{23}^{(2)}(\Delta_p - \Delta_{c1})}{A} \\
&\quad + \frac{2\Omega_p(\rho_{33}^{(2)} - \rho_{00}^{(2)})(\Delta_p - \Delta_{c1})(\Delta_p - \Delta_{c2})}{A}
\end{aligned} \tag{4}$$

$$\begin{aligned}
A &= (\Delta_p - \Delta_{c2})[4(i\gamma_{03} - \Delta_p)(\Delta_p - \Delta_{c1}) + \Omega_{c1}^2] \\
&\quad + \Omega_{c2}^2(\Delta_p - \Delta_{c1})
\end{aligned} \tag{5}$$

By using the relation between polarization and electric field, the 1st and 3rd-order susceptibilities ($\chi^{(1)}$ and $\chi^{(3)}$) of the probe laser field, with the density of four level systems N, can are obtained as follows:

$$\chi^{(1)}(\omega_p) = \frac{2\,N\,|\hat{\vec{\mu}}_{03}|^2}{\varepsilon_0\,\hbar\,\Omega_p}\rho_{03}^{(1)} \tag{6}$$

$$\chi^{(3)}(\omega_p) = \frac{2\,N\,|\hat{\vec{\mu}}_{03}|^4}{3\,\varepsilon_0\,\hbar^3\,\Omega^3{}_p}\rho_{03}^{(3)} \tag{7}$$

and the effective susceptibility $\chi_{eff}(\omega_p)$ is defined as:

$$\chi_{eff}(\omega_p) = \chi^{(1)}(\omega_p) + 3\chi^{(3)}(\omega_p)\,|\vec{E}(\omega_p)|^2 \tag{8}$$

The refractive index of the probe laser field can be determined via the following relation:

$$n(\omega_p) = \sqrt{1 + \chi_{eff}(\omega_p)} \tag{9}$$

Nonlinear refractive index by using equations (6)–(8), and the Taylor expansion ($\chi_{eff}(\omega_p) \ll 1$) can be written as:

$$n(\omega_p) = n_0(\omega_p) + \frac{3\ \mathrm{Re}\,\chi^{(3)}(\omega_p)}{2n_0(\omega_p)}\,|\vec{E}(\omega_p)|^2 \tag{10}$$

Here the fifth order term is neglected, due to its small effect. $n_0(\omega_p)$ is the linear refractive index which related to $\mathrm{Re}\,\chi^{(1)}(\omega_p)$ as follows:

$$n_0(\omega_p) = 1 + \frac{1}{2}\,\mathrm{Re}\,\chi^{(1)}(\omega_p) \tag{11}$$

$\vec{E}(\omega_p)$ in equation (10) is related to the intensity of the probe laser field as:

$$I(\omega_p) = 2n_0(\omega_p)\varepsilon_0 c\,|\vec{E}(\omega_p)|^2 \tag{12}$$

where c is the velocity of light in vacuum. So, the nonlinear refractive index can be obtained as:

$$n(\omega_p) = n_0(\omega_p) + n_2(\omega_p)I(\omega_p) \tag{13}$$

where $n_2(\omega_p)$ ($n_2(\omega_p) = 3\,\mathrm{Re}\,\chi^{(3)}(\omega_p)/4\,n_0^2(\omega_p)\varepsilon_0\,c$) is Kerr nonlinear, which related to $\mathrm{Re}\,\chi^{(3)}(\omega_p)$. The group velocity ($v_g$) of the probe laser field is related to the slope of the dispersion as follows:

$$v_g(\omega_p) = \frac{c}{n(\omega_p) + \omega_p\frac{dn(\omega_p)}{d\omega_p}} \tag{14}$$

The group index, $n_g(\omega_p)$, is determined by:

$$n_g(\omega_p) = n(\omega_p) + \omega_p\frac{dn(\omega_p)}{d\omega_p} \tag{15}$$

To replace equation (13) in equation (15), linear group index (n_{lg}) and 3rd-order nonlinear group index (n_{nlg}) of the probe laser field can be written:

$$n_{lg}(\omega_p) = n_0(\omega_p) + \omega_p\frac{dn_0(\omega_p)}{d\omega_p} \tag{16}$$

$$n_{nlg}(\omega_p) = n_2(\omega_p)I(\omega_p) + \omega_p\frac{d(n_2(\omega_p)I(\omega_p))}{d\omega_p} \tag{17}$$

So, the final expression of the linear group velocity (v_{lg}) and 3rd-order nonlinear group velocity (v_{nlg}) of the probe laser field are given by:

$$v_{lg}(\omega_p) = \frac{c}{n_{lg}(\omega_p)} \tag{18}$$

$$v_{nlg}(\omega_p) = \frac{c}{n_{lg}(\omega_p) + n_{nlg}(\omega_p)} \tag{19}$$

In order to investigate linear and 3rd-order nonlinear group velocities, it is essential to obtain μ_{03}, μ_{13} and μ_{23} because the eigenstates of matter and polarization vector of lasers depend on them.

3. Cylindrical quantum dot

The Hamiltonian of cylindrical QD with the length L and radius R, with parabolic potential, in the effective-mass approximation, is given by:

$$H_\circ = -\frac{\hbar^2}{2m_e^*}\nabla^2 + \frac{1}{2}m_e^*\omega_{\circ\rho}^2\rho^2 + \frac{1}{2}m_e^*\omega_{\circ z}^2 z^2 \tag{20}$$

where m_e^* is the electron effective- mass, $\omega_{0\rho} = \hbar^2/m_e^* R^2$ and $\omega_{0z} = 4\hbar^2/m_e^* L^2$ illustrates the electron oscillation frequencies in directions of R and L of cylindrical QD, respectively. Eigenfunction of $H_\circ$ is calculated as:

$$\psi_{n_1 n_2 n_3}(x_1, x_2, x_3) = \sqrt{\frac{k_z {k_\rho}^2}{n_1! n_2! n_3! 2^{n_1+n_2+n_3}\sqrt{\pi}}}\, e^{-\frac{1}{2}(x_1^2+x_2^2+x_3^2)} H_{n_1}(x_1) \times H_{n_2}(x_2) H_{n_3}(x_3) \tag{21}$$

Where $k_\rho = \sqrt{m_\circ^* \omega_{\circ\rho}/\hbar}$ and $k_z = \sqrt{m_\circ^* \omega_{\circ z}/\hbar}$ are defined effective wave numbers, n_1, n_2 and n_3 are quantum numbers and $H_n(x)$ is the Hermit polynomials and eigenkets are shown by $|n_1 n_2 n_3\rangle$. The eigenvalues of $H_\circ$ is also given by:

$$E^0_{n_1 n_2 n_3} = (n_1 + n_2 + 1)\hbar\omega_{0\rho} + \left(n_3 + \frac{1}{2}\right)\hbar\omega_{0z} \tag{22}$$

It is essential to select polarization vector of lasers and four levels of $|0\rangle$, $|1\rangle$, $|2\rangle$ and $|3\rangle$ in order to calculate the μ_{03}, μ_{13} and μ_{23}. Eigenfunctions of $H_\circ$ have a definite parity, since Hamiltonian operator $\widehat{H_\circ}$ commutes with parity operator $\hat{\pi}$ ($[\widehat{H_\circ}, \hat{\pi}] = 0$). In this system, parity of eigenfunctions is determined by evenness or oddness of quantum numbers n_1, n_2, and n_3. By choosing $|0\rangle = |000\rangle$, $|1\rangle = |002\rangle$, $|2\rangle = |004\rangle$ as even parity and $|3\rangle = |005\rangle$ as odd parity and polarization of laser beams along Z axis QD ($\vec{E} = E\ \hat{e}_z$), the elements of dipole moment in allowed transitions are obtained as:

$$\mu^z_{(000)(005)}(R, L) = -\frac{(-1 + e^{a^2k_\rho^2})\, L^3 k_z^2\, e\, e^{-\frac{1}{4}L^2k_z^2 - a^2k_z^2}}{16\sqrt{15\pi}}(-10 + L^2k_z^2) \tag{23}$$

$$\mu^z_{(002)(005)}(R, L) = -\frac{(-1 + e^{a^2k_\rho^2})\, L^3 k_z^2\, e\, e^{-\frac{1}{4}L^2k_z^2 - a^2k_\rho^2}}{32\sqrt{30\pi}} \times (-20 - 8L^2k_z^2 + L^4k_z^4) \tag{24}$$

$$\mu^z_{(004)(005)}(R, L) = -\frac{(-1 + e^{a^2k_\rho^2})\, L^3 k_z^2\, e\, e^{-\frac{1}{4}L^2k_z^2 - a^2k_\rho^2}}{384\sqrt{10\pi}\, k_z} \times (-1920 e^{\frac{1}{4}L^2k_z^2}\sqrt{\pi}\, Erf\left(\frac{1}{2}Lk_z\right) + 1920Lk_z + 200L^3k_z^3 + 116L^5k_z^5 - 14L^7k_z^7 + L^9k_z^9) \tag{25}$$

where $erf(x)$ is the error function. By choosing $|0\rangle = |000\rangle$, $|1\rangle = |200\rangle$, $|2\rangle = |400\rangle$ and $|3\rangle = |500\rangle$ and lasers' polarization vector in direction of radius of QD ($\vec{E} = E\ \hat{e}_x$) the elements of dipole moment for allowed transitions are obtained as:

$$\mu^x_{(000)(500)}(R, L) = -\frac{e\, a^4\, e^{-a^2k_\rho^2}}{8}\sqrt{\frac{5}{3}}\, Erf\left(\frac{1}{2}Lk_z\right) \times k_\rho^3(-3 + a^2k_\rho^2) \tag{26}$$

$$\mu^x_{(200)(500)}(R, L) = -\frac{e\, a^4\, e^{-a^2k_\rho^2}}{32}\sqrt{\frac{5}{6}}\, Erf\left(\frac{1}{2}Lk_z\right)k_\rho^3 \tag{27}$$

$$\mu^x_{(400)(500)}(R, L) = \frac{e\, Erf\left(\frac{1}{2}Lk_z\right)}{192\sqrt{10}\, k_\rho} \times (-960 - e^{-a^2k_\rho^2}(960 + a^2k_\rho^2(960 + 300a^2k_\rho^2 + 580a^4k_\rho^4 - 245a^6k_\rho^6 + 63a^8k_\rho^8))) \tag{28}$$

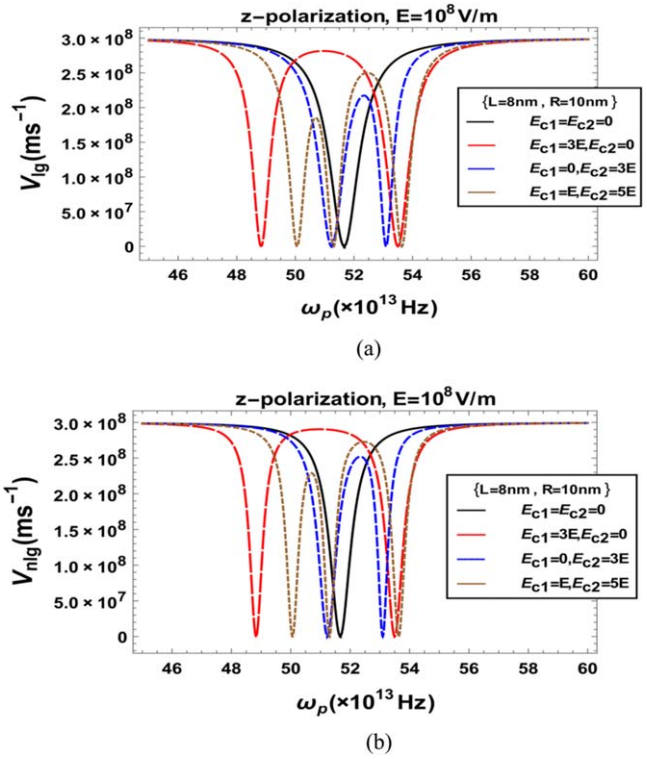

Figure 2. The diagram of the (a) linear group velocity (v_{lg}) and (b) 3rd-order nonlinear group velocity (v_{nlg}) under z-polarization with $L = 8$ nm and $R = 10$ nm for four different cases $E_{c1} = E_{c2} = 0$, $E_{c1} = 3 \times 10^8$ v m^{-1}, $E_{c2} = 0$, $E_{c1} = 0$, $E_{c2} = 3 \times 10^8$ v m^{-1} and $E_{c1} = 10^8$ v m^{-1}, $E_{c2} = 5 \times 10^8$ v m^{-1}.

4. Results and discussions

In this section, linear and 3rd-order nonlinear group velocities (v_{lg}, v_{nlg}) are investigated by using EIT in a TTFLCQD, as shown in figure 1(a). For simplicity and convenience, all the parameters are set with $\gamma_{03} = 10^{11}s^{-1}$; $\gamma_{23} = \gamma_{13} = \Gamma_{03} = \Gamma_{13} = \Gamma_{23} = \gamma_{03}$, $\Delta_{c1} = 10^2\gamma_{03}$, $\Delta_{c2} = -10^2\gamma_{03}$ and $\gamma_{01} = \gamma_{12} = \gamma_{02} = 10^{-4}\gamma_{03}$. Figure 2 is illustrated linear and 3rd-order

Table 1. The values of ω_p (Hz), $\Delta\omega_p$, $(v_{l\ g})^{\max}(ms^{-1})$ and $(v_{nl\ g})^{\max}(ms^{-1})$ for figures 2(a) and (b) with L = 8(nm), R = 10(nm), $E_c = 10^8$(v m^{-1}) for four different cases $E_{c1} = E_{c2} = 0$, $E_{c1} = 3E_c$, $E_{c2} = 0$, $E_{c1} = 0$, $E_{c2} = 3E_c$ and $E_{c1} = E_c$, $E_{c2} = 5E_c$ under z-polarization, R = 10(nm).

Z-polarization						
$E_c = 10^8$(v m^{-1})		L = 8(nm)		$\omega_p \times 10^{13}$(Hz)		
$\Delta p \times 10^{13}$						
	Left	Center	Right	Left	Center	Right
$E_{c1} = E_{c2} = 0$	—	51.674	—	—	—	—
$E_{c1} = 0$, $E_{c2} = 3E_c$	51.24	—	53.099	—	1.859	—
$E_{c1} = 3E_c$, $E_{c2} = 0$	48.827	—	53.504	—	4.677	—
$E_{c1} = E_c$, $E_{c2} = 5E_c$	50.062	51.313	53.628	1.251	—	2.315
	$(v_{l\ g})^{\max} \times 10^8$ (ms^{-1})			$(v_{nl\ g})^{\max} \times 10^8$ (ms^{-1})		
$E_{c1} = E_{c2} = 0$	—	—	—	—	—	—
$E_{c1} = 0$, $E_{c2} = 3E_c$	—	2.172	—	—	2.52	—
$E_{c1} = 3E_c$, $E_{c2} = 0$	—	2.814	—	—	2.9	—
$E_{c1} = E_c$, $E_{c2} = 5E_c$	1.852	—	2.501	2.29	—	2.728

nonlinear group velocities versus $\omega_p \times 10^{13}$ Hz with L = 8 nm and R = 10 nm for z-polarization in the presence and absence of the control laser fields. By analyzing figure 2 it is seen, when both the control laser fields E_{c1} and E_{c2} are off ($E_{c1} = E_{c2} = 0$) the linear and 3rd-order nonlinear group velocities are minimized at frequency 51.6748×10^{13} Hz and light is absorbed by the system at the same frequency. By applying one of the control laser fields ($E_{c1} = 3 \times 10^8$ v m^{-1}, $E_{c2} = 0$ or $E_{c1} = 0$, $E_{c2} = 3 \times 10^8$ v m^{-1}), $v_{l\,g}$ and $v_{nl\,g}$ at two frequencies are minimized. Also, the light at the same frequencies is absorbed. It can also be seen from figure 2, that one slow light frequency range ($\Delta\omega_p$) is created, which be seen at the center of $v_{l\,g}$ and $v_{nl\,g}$ curves $(\Delta\omega_p)_C$. In other words, one transparency window is created. Pay attention to figure 2, it is observed that in the presence of both control laser fields ($E_{c1} = 10^8$ v m^{-1}, $E_{c2} = 5 \times 10^8$ v m^{-1}), $v_{l\,g}$ and $v_{nl\,g}$ at three frequencies 53.6297×10^{13} Hz, 51.3074×10^{13} Hz and 50.0533×10^{13} Hz are minimized. Also, two slow light frequency ranges are created; one is on the right-hand side of $v_{l\,g}$ and $v_{nl\,g}$ curves $(\Delta\omega_p)_R$ and the other is on the left-hand side of $v_{l\,g}$ and $v_{nl\,g}$ curves $(\Delta\omega_p)_L$. The numerical results of figure 2 are listed in table 1. $(\omega_p)_R$, $(\omega_p)_C$, and $(\omega_p)_L$ in table 1 are defined as the right, center and left frequencies of the $v_{l\,g}$ and $v_{nl\,g}$ curves, respectively. Base on the results of table 1, it is found that $(\Delta\omega_p)_C$ for case $E_{c1} = 3 \times 10^8$ v m^{-1}, $E_{c2} = 0$ is wider than the case $E_{c1} = 0$, $E_{c2} = 3 \times 10^8$ v m^{-1}. In addition, $(v_{l\,g})^{\max}$ and $(v_{nl\,g})^{\max}$ that are defined as maximum values of $v_{l\,g}$ and $v_{nl\,g}$ at slow light frequency ranges, for case $E_{c1} = 3 \times 10^8$ v m^{-1}, $E_{c2} = 0$ are more than the case $E_{c1} = 0$, $E_{c2} = 3 \times 10^8$ v m^{-1}. As can be seen clearly from figure 2 and table 1 that for case $E_{c1} = 10^8$ v m^{-1}, $E_{c2} = 5 \times 10^8$ v m^{-1}, $(\Delta\omega_p)_R$ gets wider than $(\Delta\omega_p)_L$. Also, $(v_{l\,g})^{\max}$ and $(v_{nl\,g})^{\max}$ at the right-hand side of $v_{l\,g}$ and $v_{nl\,g}$ curves $((v_{l\,g})^{\max}_R, (v_{nl\,g})^{\max}_R)$ are larger than $(v_{l\,g})^{\max}$ and $(v_{nl\,g})^{\max}$ at the left-hand side of $v_{l\,g}$ and $v_{nl\,g}$ curves $((v_{l\,g})^{\max}_L, (v_{nl\,g})^{\max}_L)$.

4.1. Comparison of linear and 3rd-order nonlinear group velocities

Figure 3 is plotted in order to compare the linear and 3rd-order nonlinear group velocities with $E_{c1} = 10^8$ v m^{-1} and $E_{c2} = 5 \times 10^8$ v m^{-1} at z-polarization. It can be seen from figure 3 that both $v_{l\,g}$ and $v_{nl\,g}$ at three frequencies 53.6297×10^{13} Hz, 51.3074×10^{13} Hz, and 50.0533×10^{13} Hz are minimized. In addition, $(\Delta\omega_p)_L$ for $v_{l\,g}$ and $v_{nl\,g}$ and also $(\Delta\omega_p)_R$ for $v_{l\,g}$ and $v_{nl\,g}$ are equal, i.e., $(\Delta\omega_p)_L^{v_{l\,g}} = (\Delta\omega_p)_L^{v_{nl\,g}}$ and $(\Delta\omega_p)_R^{v_{l\,g}} = (\Delta\omega_p)_R^{v_{nl\,g}}$. It is also observed that maximum values of 3rd-order nonlinear group velocity are more than linear group velocity at slow light frequency ranges.

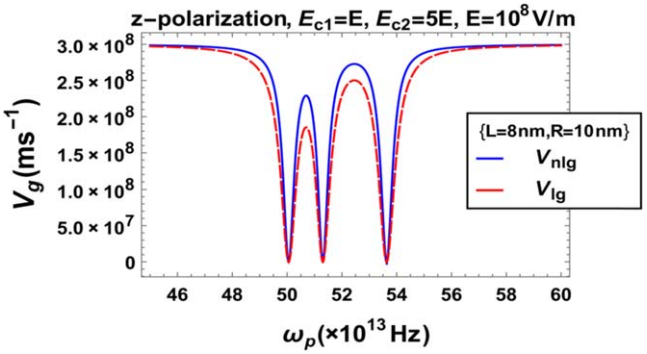

Figure 3. Linear and 3rd-order nonlinear group velocities with L = 8 nm, R = 10 nm and $E_{c1} = 10^8$ v m^{-1}, $E_{c2} = 5 \times 10^8$ v m^{-1} under z-polarization.

4.2. Effects of parameters of cylindrical QD

To illustrate the effects of parameters of cylindrical QD (L and R) on 3rd-order nonlinear and linear group velocities figure 4 is plotted. Figure 4(a) is shown $v_{nl\,g}$ for two different values of the length of cylindrical QD (L) at z-polarization. It can be seen that by increasing L, curve of $v_{nl\,g}$ is moved towards lower frequencies (red shift), because when polarization vector of lasers are in the direction of the length of QD (z-direction), by changing L, the electron oscillation frequency in direction of length of cylindrical QD is changed. Also, $(\Delta\omega_p)_R$ and $(\Delta\omega_p)_L$ become wider with increasing L. Besides, the values of $(v_{nl\,g})^{\max}$ are increased by increasing L.

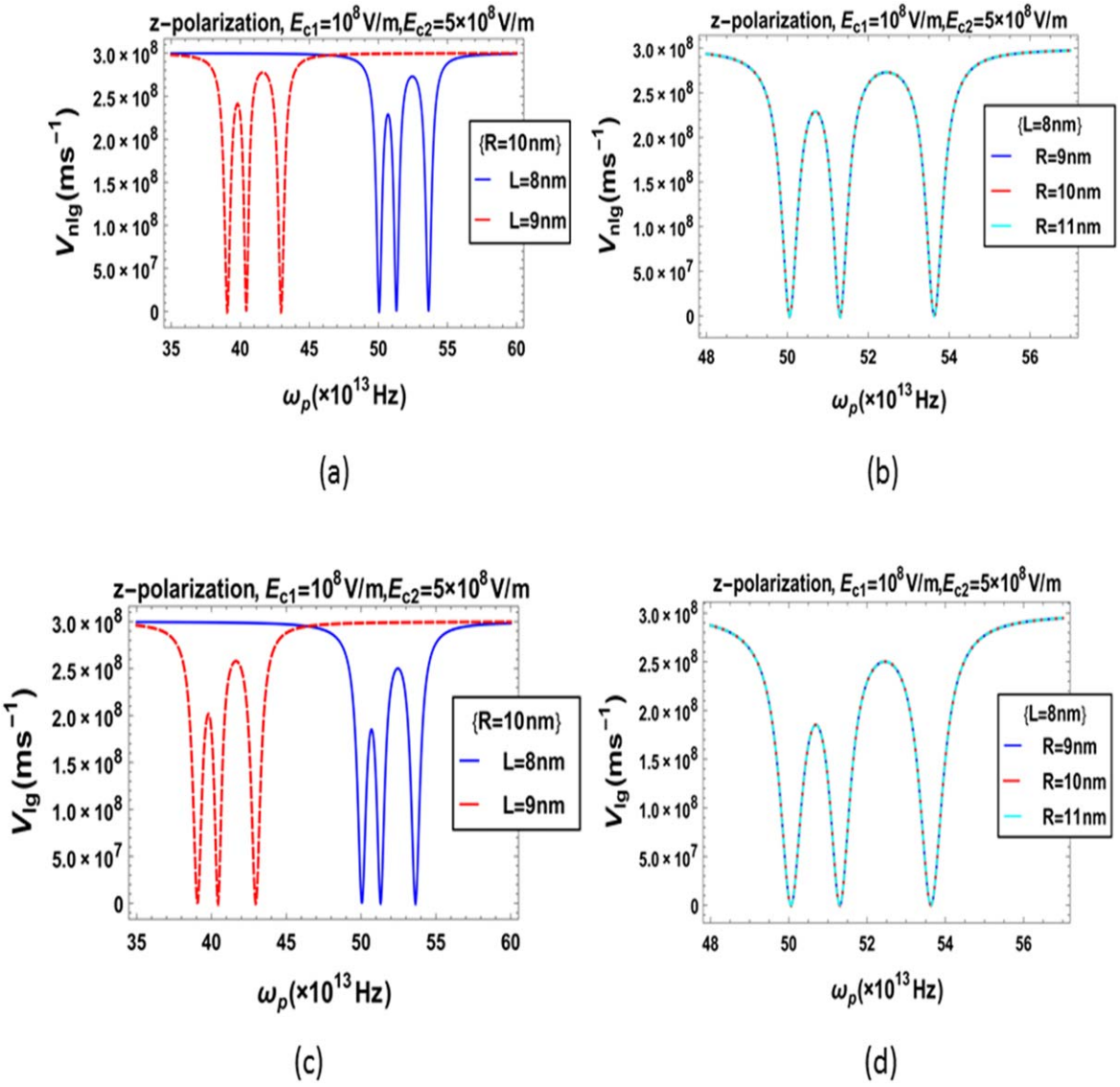

Figure 4. The diagram of the (a) 3rd-order nonlinear group velocity with R = 10 nm at two different lengths (L) of cylindrical QD, (b) 3rd-order nonlinear group velocity at L = 8 nm and three different radiuses (R) of cylindrical QD, (c) linear group velocity with R = 10 nm at two different lengths (L) of cylindrical QD, (d) linear group velocity with L = 8 nm at three different radiuses (R) of cylindrical QD under z-polarization.

Table 2. The values of ω_p (Hz), $\Delta\omega_p$, and $(v_{nl\ g})^{max}(ms^{-1})$ for two different lengths of cylindrical QD in figure 4(a) with R = 10(nm), $E_{c1} = 10^8(v\ m^{-1})$ and $E_{c2} = 5E_{c1}$ under z- polarization.

Z-polarization						
	$\omega_p \times 10^{13}$(Hz)			$\Delta\omega_p \times 10^{13}$		
$L = 8$ nm	Left	Center	Right	Left	Center	Right
$L = 9$ nm	50.062	51.313	53.628	1.251	—	2.315
	39.073	40.443	42.968	1.37	—	2.525
	$(v_{nl\ g})^{max} \times 10^8\ (ms^{-1})$					
$L = 8$ nm		Left		Center		Right
$L = 9$ nm		2.29		—		2.728
		2.410		—		2.773

The results of figure 4(a) are summarized in table 2. It is understood from figure 4(b) that the 3rd-order nonlinear group velocity is not dependent on the radius of cylindrical QD (R) in z-polarization, because electrons have no oscillation in the x-direction, due to polarization vector of lasers are in the z-direction. In figures 4(c) and (d), v_{lg} for different values of L and R in z-polarization, are plotted. Based on the results of figure 3, it is obvious that the effects

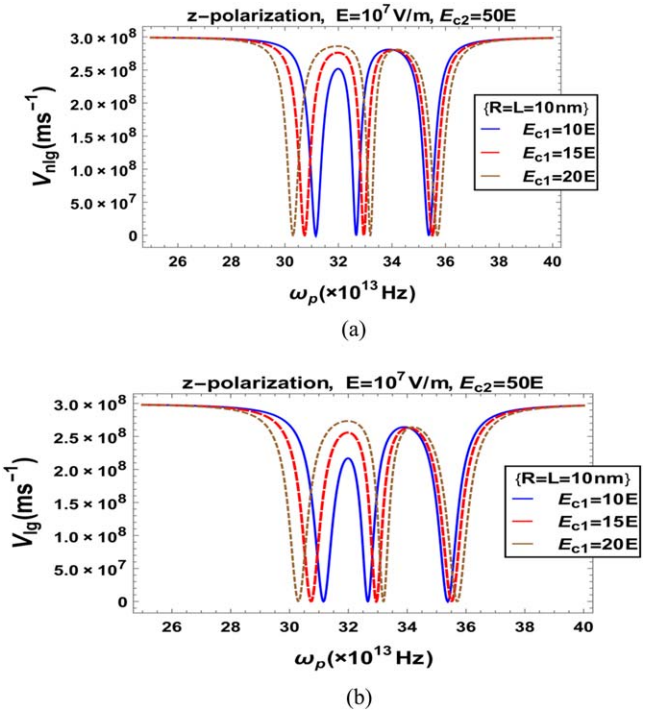

Figure 5. The diagram of the (a) 3rd-order nonlinear group velocity, and (b) linear group velocity with R = L = 10 nm for three different E_{c1} under z-polarization.

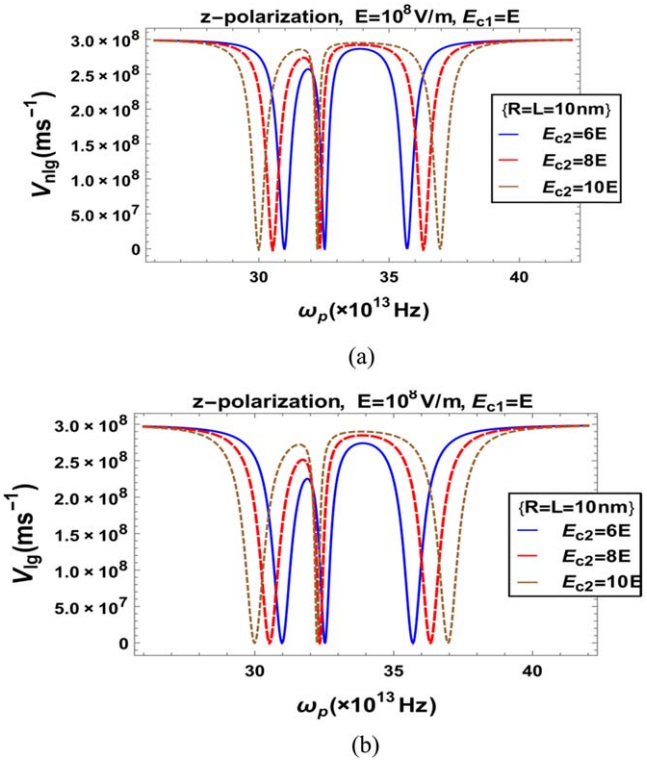

Figure 6. The diagram of the (a) 3rd-order nonlinear group velocity, and (b) linear group velocity with L = R = 10 nm for three different E_{c2} under z-polarization.

of L and R of cylindrical QD on linear group velocity are the same with the 3rd-order nonlinear group velocity.

4.3. Effects of the control laser fields

In figure 5(a) $v_{nl\,g}$ in terms of $\omega_p \times 10^{13}$ Hz with three different values of E_{c1} and R = L = 10 nm in z-polarization is displayed. It can be seen that with increasing E_{c1}, $(\omega_p)_R$ and $(\omega_p)_c$ are shifted toward higher frequencies (blue shift) and $(\omega_p)_L$ is shifted toward lower frequency (red shift). Moreover, the width of $(\Delta\omega_p)_R$ and $(\Delta\omega_p)_L$ are increased and decreased by increasing E_{c1}, respectively. From figure 5(a), it can be discerned that by increasing E_{c1}, the value of $(v_{nl\,g})_R^{\max}$ at frequency 34.05 $\times$ 10^{13} Hz does not change, but the value of $(v_{nl\,g})_L^{\max}$ at frequency 31.98 $\times$ 10^{13} Hz is increased. Figure 5(b) is shown the changes of $v_{l\,g}$ versus $\omega_p \times 10^{13}$ Hz, when E_{c1} is increased. According to the results of figure 3, the effects of E_{c1} on linear group velocity are similar to 3rd-order nonlinear group velocity.

The 3rd-order nonlinear group velocity versus $\omega_p \times 10^{13}$ Hz with three various values of E_{c2} when other parameters are constant for z-polarization is plotted in figure 6(a). It is observed by increasing E_{c2} blue shift for $(\omega_p)_R$ and red shift for $(\omega_p)_L$ and $(\omega_p)_C$ are occurred. Also, with increasing E_{c2}, $(\Delta\omega_p)_R$ and $(\Delta\omega_p)_L$ are wider. In addition, from figure 6(a) it is found that increasing E_{c2}, $(v_{nl\,g})_R^{\max}$ and $(v_{nl\,g})_L^{\max}$ are increased. Figure 6(b) is represented linear group velocity in terms of $\omega_p \times 10^{13}$ Hz with three different values of E_{c2} when other parameters are constant in z-polarization. All results of figure 6(a), for figure 6(b) are also true, due to the results of figure 3.

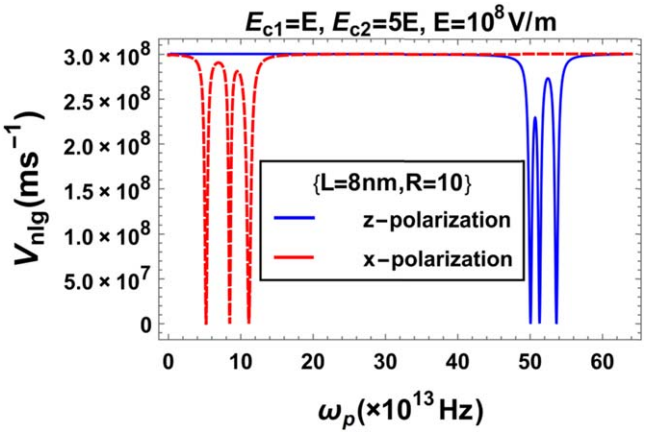

Figure 7. The 3rd-order nonlinear group velocity with L = 8 nm, R = 10 nm, $E_{c1} = 10^8$ v m^{-1} and $E_{c2} = 5 \times 10^8$ v m^{-1} under x-polarization and z-polarization.

4.4. Comparison of x-polarization and z-polarization

The 3rd-order nonlinear group velocity for x- and z-polarization is compared in figure 7. Investigation on

figure 7 is shown that $v_{nl\,g}$ in x-polarization at smaller frequencies than z-polarization is minimized. $(\Delta\omega_p)_R$ and $(\Delta\omega_p)_L$ in x-polarization are wider than z-polarization. For x-polarization, the value of $(v_{nl\,g})_R^{\max}$ is smaller than the value of $(v_{nl\,g})_L^{\max}$, but for z-polarization, the value of $(v_{nl\,g})_R^{\max}$ is greater than the value of $(v_{nl\,g})_L^{\max}$.

5. Conclusion

In this paper, the linear and 3rd-order nonlinear group velocities ($v_{l\,g}$, $v_{nl\,g}$) in a TTFLCQD in electromagnetically induced transparency phenomenon are investigated. The results are shown that there is one slow light frequency range when one of the control laser fields is applied on cylindrical QD, and in the presence of both control laser fields, two slow light frequency ranges are created. The linear and 3rd-order nonlinear group velocities are minimized at the same frequencies, but maximum values of the 3rd-order nonlinear group velocity are more than the linear group velocity. For z-polarization, by increasing length of cylindrical QD (L), $(v_{nl\,g})^{\max}$ and $(v_{l\,g})^{\max}$ are increased and $(\Delta\omega_p)_R$ and $(\Delta\omega_p)_L$ become wider. But $v_{nl\,g}$ and $v_{l\,g}$ are not dependent on the radius of cylindrical QD in z-polarization. By increasing E_{c1}, $(\Delta\omega_p)_R$ and $(\Delta\omega_p)_L$ become wider and closer, respectively. With increasing E_{c2}, the width of $(\Delta\omega_p)_R$ and $(\Delta\omega_p)_L$ are increased. $(\Delta\omega_p)_R$ and $(\Delta\omega_p)_L$ in x-polarization are wider than z-polarization. Moreover, the blue shift and red shift are occurred by increasing L, E_{c1} and E_{c2}.

ORCID iDs

Mohammad Reza Rezaie https://orcid.org/0000-0003-2392-0662
Hassan Ranjbar Askari https://orcid.org/0000-0001-9817-0988

References

[1] Boyd R W and Gauthier D J 2009 Controlling the velocity of light pulses *Science* **326** 1074–7
[2] Milonni P W 2002 Controlling the speed of light pulses *J. Phys. B: At. Mol. Opt. Phys.* **35** R31–56
[3] Harris S E and Hau L H 1999 Nonlinear optics at low light levels *Phys. Rev. Lett.* **82** 4611
[4] Beausoleil R G, Munro W J, Rodrigues D A and Spiller T P 2004 Applications of electromagnetically induced transparency to quantum information processing *J. Mod. Opt.* **51** 2441–8
[5] Zhang S, Zhou S, Loy M M T, Wong G K L and Du S 2011 Optical storage with electromagnetically induced transparency in a dense cold atomic ensemble *Opt. Lett.* **36** 4530–2
[6] Harris S E and Yamamoto Y 1998 Photon switching by quantum interference *Phys. Rev. Lett.* **81** 3611
[7] Ku P C, Chang-Hasnain C J and Chuang S L 2002 Variable semiconductor all-optical buffer *Electron. Lett.* **38** 1581–3
[8] Hua X, Liu L and Zhang X 2015 Dispersion and absorption properties of the Y-type-four-level system with electromagnetically induced transparency *Opt.* **126** 172–5
[9] Wang T, Rajapakse R and Yelin S F 2007 Electromagnetically induced transparency and slow light with n-doped GaAs *Opt. Commun.* **272** 154–60
[10] Li C, Huang L, Wang W, Ma X, Zhou S and Jiang Y 2015 Electromagnetically induced transparency in nano-structures made from metallic nanorod and split-ring-resonator *Opt. Commun.* **355** 337–41
[11] Harris S E, Field S E and Imamoglu F A 1990 Nonlinear optical processes using electeromagnetically induced transparency *Phys. Rev. Lett.* **64** 1107
[12] Askari H R and Moezzi M 2015 The generation of the double windows of EIT in W-type 4-level cylindrical quantum dot *Opt.* **126** 4612–20
[13] Usefzadeh S and Karimi M J 2016 Electromagnetically induced transparency in the strained quantum wells: Effects of structural parameters and geometrical size *Opt.* **127** 10208–15
[14] Zhao Y, Zhao H W, Zhang X Y, Yuan B and Zhang S 2009 New mechanisms of slow light and their applications *Opt. Laser Technol.* **41** 517–25
[15] Kasapi A, Jain M, Yin G Y and Harris S E 1995 Electromagnetically induced transparency: propagation dynamics *Phys. Rev. Lett.* **74** 2447
[16] Hau L V, Harris S E, Dutton Z and Behroozi C H 1999 Light speed reduction to 17 metres per second in an ultracold atomic gas *Nature* **397** 594
[17] Evangelou S, Yannopapas V and Paspalakis E 2012 Transparency and slow light in a four-level quantum system near a plasmonic nanostructure *Phys. Rev. A* **86** 053811
[18] Yan W, Wang T, Li X M and Jin Y J 2012 Electromagnetically induced transparency and theoretical slow light in semiconductor multiple quantum wells *Appl. Phys. B* **108** 515–9
[19] Mirzaei M, Askari H R and Raki Z 2014 Group velocity of light in V and Λ-types cylindrical quantum dots with electromagnetically induced transparency, Superlattice *Microst.* **74** 61–9
[20] Sahebi E, Askari H R and Behroozian B 2019 Triple transparency windows in C-four level cylindrical quantum dot *Opt.* **185** 339–50
[21] Choupanzadeh B, Kaatuzian H and Kohandani R 2018 Analysis of the influence of geometrical dimensions and external magnetic field on optical properties of InGaAs/GaAs quantum-dot slow light devices *Quantum Electron.* **48** 582–8
[22] Zamani A, Setareh F, Azargoshasb T and Niknam E 2018 Spin–orbit coupling and applied magnetic field effects on electromagnetically induced transparency of a quantum ring at finite temperature *Superlattice. Microst.* **115** 40–52
[23] Lunnemann P and Mørk J 2009 Reducing the impact of inhomogeneous broadening on quantum dot based electromagnetically induced transparency *Appl. Phys. Lett.* **94** 071108
[24] Chen H J 2018 Auxiliary-cavity-assisted vacuum Rabi splitting of a semiconductor quantum dot in a photonic crystal nanocavity, Photon *Res.* **6** 1171–6
[25] Chen H J 2020 Fano resonance induced fast to slow light in a hybrid semiconductor quantum dot and metal nanoparticle system *Laser Phys. Lett.* **17** 025201
[26] Hatef A, Sadeghi S M and Singh M R 2012 Plasmonic electromagnetically induced transparency in metallic

nanoparticle–quantum dot hybrid systems *Nanotechnology* **23** 065701

[27] Kosionis S G, Terzis A F, Sadeghi S M and Paspalakis E 2012 Optical response of a quantum dot–metal nanoparticle hybrid interacting with a weak probe field *J. Phys. Condens. Matter* **25** 045304

[28] Lu Z and Zhu K D 2008 Slow light in an artificial hybrid nanocrystal complex *J. Phys. B: At. Mol. Opt. Phys.* **42** 015502

[29] Li H, Zhang H, Sun H, Hu X, Sun D and Li X 2017 Multiple spontaneously generated coherence and phase control of optical bistability and multistability in a tripod four-level atomic medium *App. Opt.* **56** 4995–5002

[30] Behroozian B and Askari H R 2018 Kerr nonlinearity and nonlinear absorption coefficient in a four-level M-model cylindrical quantum dot under the phenomenon of electromagnetically induced transparency *Laser Phys.* **28** 075401